JOURNAL OF Materials CHEMISTRY

Synthesis of mesoporous silica spheres under quiescent aqueous acidic conditions

Hong Yang, Gregory Vovk, Neil Coombs, Igor Sokolov and Geoffrey A. Ozin*

Materials Chemistry Research Group, Chemistry Department, University of Toronto, 80 St. George Street, Toronto, Ontario, Canada M5S 3H6

A gyroid-to-sphere shape transition has been unveiled in the growth of mesoporous silica morphologies that are synthesized under quiescent acidic aqueous conditions. It can be induced by a decrease of the acidity for a surfactant-based gyroid preparation. As the acidity is gradually lowered from the gyroid domain, the growth process changes from one involving a smooth continuous deposition of silicate–surfactant micellar solute species onto specific regions of an evolving silicate liquid crystal seed, to one in which deposition instead occurs on non-specific regions of the seed. This creates multigranular gyroid morphologies which at lower acidity emerge as sphere shapes. The gyroid-to-sphere metamorphosis appears to correlate with an acidity and/or temperature dependent switch in the mode of formation, from the gyroid involving fast and local polymerization of a growing silicate liquid crystal seed, to the sphere based upon a slower and global polymerization of a silicate liquid crystal droplet. Surface tension will cause such a droplet to adopt a spherical shape, ultimately to be rigidified in the form of a mesoporous silica sphere. Comparative gyroid and sphere information is presented on synthesis-size-shape-channel plan relations, degree of orientational order of the channels, extent of polymerization of the silica, thermal stability and nitrogen adsorption properties. The ability to synthesize 1–10 μm diameter mesoporous silica spheres with a narrow sphere size and pore size distribution portends a myriad of applications in large molecule catalysis, chromatographic separations and nanocomposites.

We have recently reported a synthesis strategy for controlling the morphology of mesoporous silica over all three spatial dimensions[1–9] by using a surfactant-based supramolecular templating approach.[10–12] The method is founded upon control of the nucleation, polymerization and growth of a silicate liquid crystal seed under quiescent acidic aqueous conditions, to create mesoporous silica fibers, films, a range of low and medium curvature shapes and lithographically defined micrometer scale patterns. Synthesis–morphology–channel plan relations have been delineated through variations in reactant ratios, acidity and temperature, to favor particular architectures. These kinds of mesoporous silica morphologies represent hierarchical constructions where structural features are controlled over microscopic (<10 Å), mesoscopic (10–500 Å) and macroscopic (>500 Å) length scales (IUPAC convention).[13]

Mesoporous silica morphologies that have been obtained using the supramolecular templating approach include: (i) fibers having arc, crankshaft, toroid and spiral shapes with the channels running parallel to the axis of the fiber,[1,2] (ii) discoids and gyroids with the channels whirling around the unique rotation axis,[1,2] (iii) millimeter and micrometer size solid and hollow spheres,[14,15] (iv) supported films by solution deposition onto mica, graphite, gold and glass with the channels oriented parallel to the substrate surface,[3–5,8,16] (v) supported films by sol–gel dip-coating or spin-coating on silicon and silica,[17–19] (vi) free-standing films with a liquid crystalline channel texture grown at air/water and oil/water interfaces,[6,7,20] (vii) tubular constructs,[21] (viii) self-assembled monolayer (SAM) patterned micrometer scale designs on gold,[8] (ix) oriented growth in glass capillaries and (x) directed growth by microcapillary molding.

A great deal of earlier work has dealt with methods for controlling the morphology of various metal oxides because their form often determines their function and utility. To amplify, silica and other metal oxide spheres can be readily made by traditional sol–gel synthesis.[22–24] The spheres may be formed by assembling smaller size primary particles which have the same structure as the bulk analogue. Both dense and porous silica spheres are accessible through this approach. Hydrolysis of alkoxides in mixed alchohol–water solvent systems is commonly used. The gelation of small silica particles, with or without emulsions, can lead to silicas containing encapsulated water and solvent, which can subsequently be removed to form porous materials. Their pore size distribution is typically broad and can range from micro- to meso-pores and larger, and typically show a H2 type hysteresis loop in their isotherms.[25–27] Such hysteresis is often observed for systems with poorly defined pore sizes, shapes and textures.

In this article we report that well defined mesoporous silica spheres with a mean diameter of *ca.* 6 μm and a narrow pore size distribution can be grown by simply making our reported gyroid synthesis[1] less acidic. Moreover, by manipulating the acidity and/or temperature in this system, shape transitions from gyroid to sphere to amorphous forms, with concomitant mesostructure transformations from well ordered channels to less-ordered channels to the dense glassy state, have been observed. Information is presented concerning synthesis–size–shape–channel plan relations, degree of orientational order of the channels, extent of polymerization of the silica, thermal stability and nitrogen adsorption properties. Emphasis is placed on the acidity dependent polymerization rate of silicate liquid crystal precursors and how it contributes to the emergence of distinct mesoporous silica gyroid and sphere morphologies.

It should be noted that the synthesis paradigm described here is a natural outgrowth of the synthetic protocols for shape control of mesoporous silica[1,2] by the surfactant based supramolecular templating approach.[10,11] This synthesis of mesoporous silica spheres does have the particular advantages of not needing any specialized reagents and organic/inorganic additives, such as those used in emulsion-based approaches including the surfactant modified preparation of Stöber silica spheres.[14,15] The strategy presented here involves straightforward acidity and temperature control in an aqueous synthesis that utilizes conventional source reagents. Details of the preparation and characterization of spherical morphologies are presented with a focus on the origin of the mesoporous silica gyroid to sphere shape transition and the structure–property relation between the gyroids and spheres. Mesoporous silica

spheres are envisioned to find diverse applications in large molecule catalysis and separations, chromatographic purification of mixtures of biomolecules, and nanocomposites.

Experimental

Synthesis–shape–size relationships

Tetraethyl orthosilicate (TEOS, >99.9+%, Aldrich), cetyltrimethylammonium chloride (CTACl, 29 mass% aqueous solution, Pflatz & Bauer) and hydrochloric acid (36.5–38 mass% aqueous solution, BDH) were used as received. The synthesis of the mesoporous silica spheres is a modified version of the previously reported method that utilizes quiescent and dilute acidic conditions.[1,2] The micrometer size mesoporous silica spheres were formed at either 80 °C or room temperature but at different reactant ratios, Table 1. The mesoporous silica growth process was allowed to proceed for a period of 7–10 days under static conditions at 80 °C. The materials so formed were transferred from the vessel to a Buchner funnel and washed with deionized water using Whatman #42 filter paper. One set of reactant ratios that were employed for the sphere synthesis at 80 °C was: 100 H_2O : 0.9 HCl : 0.11 CTACl : 0.13 TEOS.

Spheres that emerged from this preparation were employed for detailed characterization. It is worthwhile mentioning that mesoporous silica gyroids were synthesized by using the same reactant ratios at room temperature and quiescent conditions.

Calcination of the gyroids and spheres was achieved by heating the sample from 25 to 540 °C at 1 °C min^{-1} in air and then holding at 540 °C for 4 h.

Control experiments were conducted with dense micrometer-sized silica spheres which were synthesized according to literature protocols.[28] Acetic acid (glacial, 99.9%) was mixed with water followed by specified amounts of TEOS in a *ca.* 5 min period. The reactant ratios were: 1 H_2O : 4 CH_3CO_2H : 4 TEOS.

The mixture was kept stirring for 10 min and then left under static conditions at room temperature for *ca.* 30 min. The product was transferred to a Buchner funnel and washed with ethanol followed by acetone.

Characterization

Powder X-ray diffraction (PXRD) data was obtained on a Siemens D-5000 diffractometer using Ni-filtered Cu-Kα radiation with $\lambda = 1.541\,78$ Å. A plexiglass sample holder was used for recording the PXRD patterns.

Scanning electron microscopy (SEM) images were obtained with a Hitachi S-4500 field emission microscope using a low acceleration voltage of 2 kV to minimize the charging of the mesoporous silica surfaces. Samples were uncoated and imaged directly.

Transmission electron microscopy (TEM) images were recorded on a Philips 430 microscope operating at an accelerating voltage of 100 kV. In order to obtain ultra-thin (*ca.* 200–500 Å) sections of the mesoporous silica morphologies they were embedded in Spurr resin, heated at 80 °C for 1 day to form a block, and cut using a Drukker diamond knife.

Atomic force microscopy (AFM) experiments were conducted on a NanoScope® III microscope (Digital Instruments, CA) using silicon integrated tip cantilevers (Park Scientific Instruments, CA) for height mode scanning of the morphologies. The cantilevers were used as received. Images of the surfaces of the mesoporous silica were obtained by using direct contact (dc) scanning mode.

Light scattering particle size analysis was conducted with a Malvern Mastersizer particle size analyzer using a 300RF lens suitable for the size range 0.05–880 μm. Particle agglomeration was minimized by mixing the samples in deionized water, which functioned as a dispersing agent, and submerging the mixtures for 5 min in an ultrasound bath. Mie scattering theory was used to fit the measured light signal to a particle size distribution.

Thermogravimetry (TG) was conducted on a Perkin Elmer Thermogravimetric Analyzer 7 Series. The samples were heated at a rate of 5 °C min^{-1} under a flow of N_2.

Adsorption isotherms were collected by a gravimetric technique using a McBain balance interfaced to a computer, Fig. 1. The sample (*ca.* 100 mg) was placed in a small quartz basket, which was suspended from a quartz spring and outgassed at 400 °C for 5 h. The entire sample tube was immersed into liquid nitrogen before data collection began. Incremental amounts of gas were slowly introduced into the system by a computer-controlled piezoelectric valve. Each point of uptake *vs.* pressure was recorded once the pressure of the system remained constant, at which point the system was in a state of equilibrium. Pressures were measured with two Baratron pressure transducers having ranges that covered 0–100 and 0–1000 Torr. The uptake of N_2 was measured by a Schaevitz linear displacement transducer, which measured the vertical displacement of an iron core suspended from the quartz spring and attached to the sample basket by a long quartz hook. The pore size distributions and the pore volumes were obtained using the Dollimore–Heal method while the surface area was obtained using the BET method.

Results and Discussion

Scanning electron microscopy (SEM) images of as-synthesized and calcined sphere morphologies that had been synthesized at 80 °C, using the reactant mole ratios, are shown in Fig. 2(A) and (B). There are no detectable changes between the shapes of the as-synthesized and calcined materials. The spheres remain intact and appear to have similar surface roughness. The surfaces of the spheres were relatively smooth when viewed at high magnification in an SEM, Fig. 2(C). By contrast, gyroid

Table 1 Several representative synthetic ranges that favor the formation of mesoporous silica spheres

		molar ratio			
sample	temperature/°C	H_2O	HCl	CTACl	TEOS
1	80	100	0.97	0.054	0.062
2	80	100	0.99	0.22	0.26
3	80	100	0.79	0.11	0.13
4	80	100	1.40	0.11	0.13
5	RT[a]	100	0.4–0.5	0.11	0.13

[a]RT = room temperature.

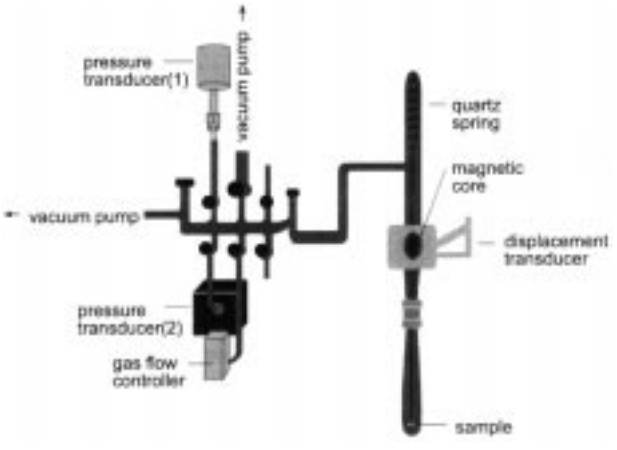

Fig. 1 Set-up of the McBain balance for adsorption isotherm measurements

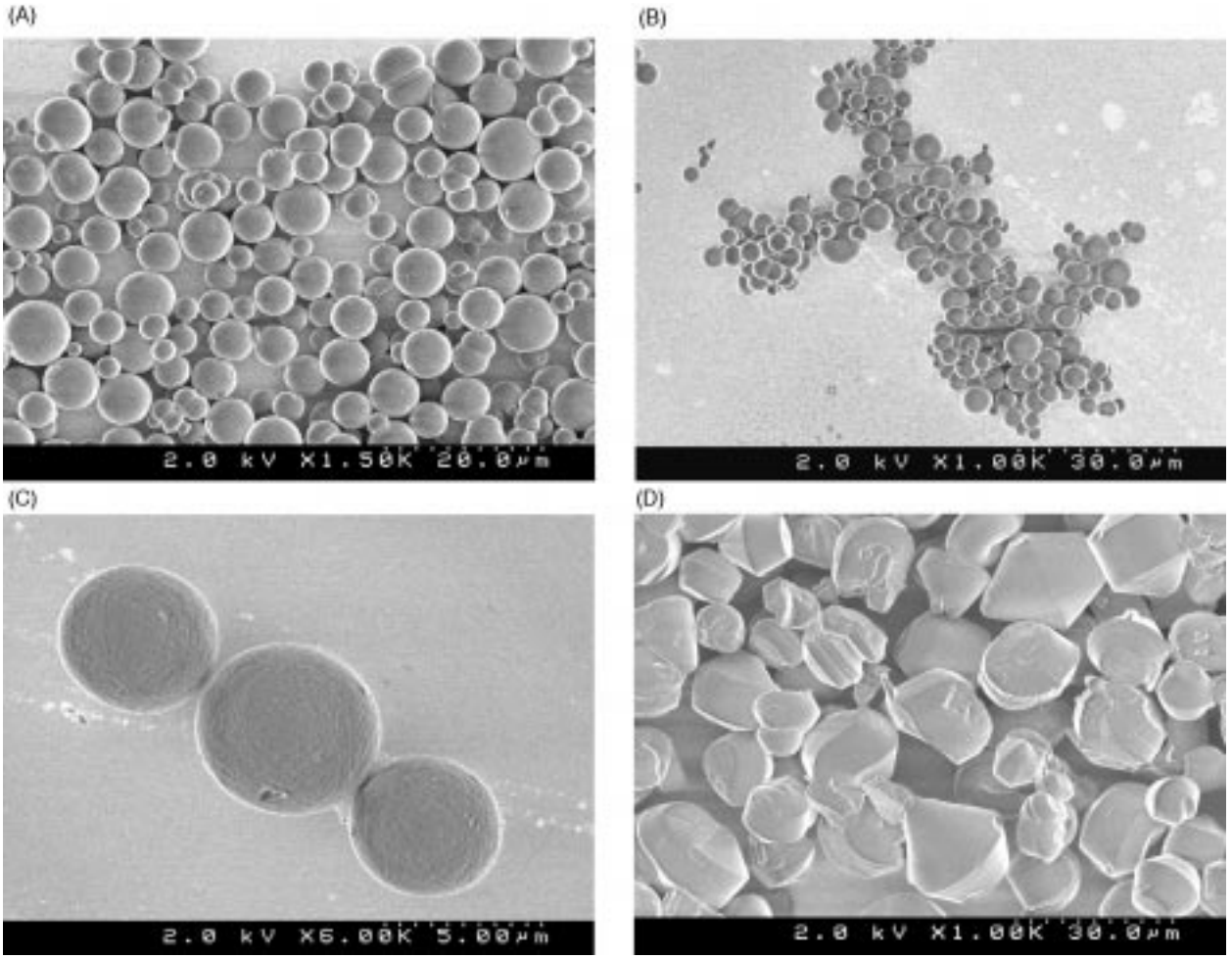

Fig. 2 Representative SEM images of synthetic silica shapes for (A) as-synthesized spheres, (B) calcined spheres, (C) spheres at high magnification and (D) gyroids made from mixture with same reactant ratio (100 H_2O : 0.9 HCl : 0.11 CTACl : 0.13 TEOS) but at different temperatures (A–C: 80 °C; D: room temperature)

shapes were obtained in a synthesis that employed the same reactant ratio but was performed at room temperature, Fig. 2(D).

The corresponding powder X-ray diffraction (PXRD) patterns are displayed in Fig. 3. A control experiment was conducted with dense micrometer-sized spheres,[28] they showed no X-ray diffraction, Fig. 3(A). The PXRD trace of as-synthesized silica spheres corresponding to those in Fig. 2(A) shows a broad low angle reflection with a *d*-spacing around 45 Å which

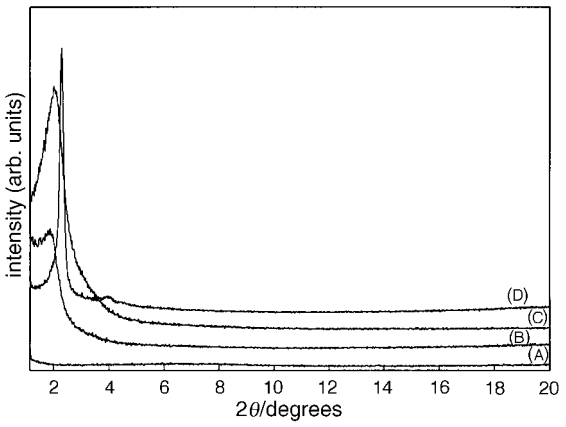

Fig. 3 Representative PXRD traces of (A) dense micron diameter silica spheres,[28] (B) as-synthesized mesoporous spheres, (C) calcined mesoporous spheres and (D) as-synthesized gyroids made from the mixture with the reactant ratio corresponding to Fig. 2

is typical for a hexagonal form of mesoporous silica with poorly ordered channels, Fig. 3(B).[29,30] The absence of high angle reflections suggests that the constitution of the silica wall is glassy. A small shift of the low angle reflection to higher 2θ for calcined silica spheres corresponds to a *ca.* 4–5 Å decrease in *d*-spacing. This is due to the condensation–polymerization of residual hydroxy groups and concomitant contraction of the pore center-to-center distance, Fig. 3(C). The considerable increase in intensity and narrowing of the PXRD peaks observed for the calcined spheres presumably arises from the improvement of the mesopore order that is induced by the combined removal of the surfactant and the ensuing condensation–polymerization reaction. Unlike the mesoporous silica spheres, the PXRD pattern of the mesoporous silica gyroids show four reflections: (100), (110), (200) and (210), that are typical of a hexagonal mesoporous silica with well ordered channels, Fig. 3(D). The PXRD trace of the gyroids shown in Fig. 2(D) displays a d_{100}-spacing of *ca.* 39 Å which is notably less than the d_{100}-spacing of *ca.* 45 Å for the spherical form of mesoporous silica. It is also noteworthy that the d_{100}-spacing of the silicate-surfactant lyotropic liquid crystal phase is reported to be *ca.* 47 Å and undergoes a polymerization induced contraction of *ca.* 4–5 Å on transforming to the mesoporous silica phase.[31] The full width at half height (FWHH) of the (100) reflection for the as-synthesized gyroid and sphere shapes is *ca.* 0.15 and 0.57° 2θ respectively, implying that the spheres have a less ordered mesopore structure than the gyroids.

Transmission electron microscopy (TEM) images (recorded from an epoxy-embedded and microtomed *ca.* 200–500 Å thin

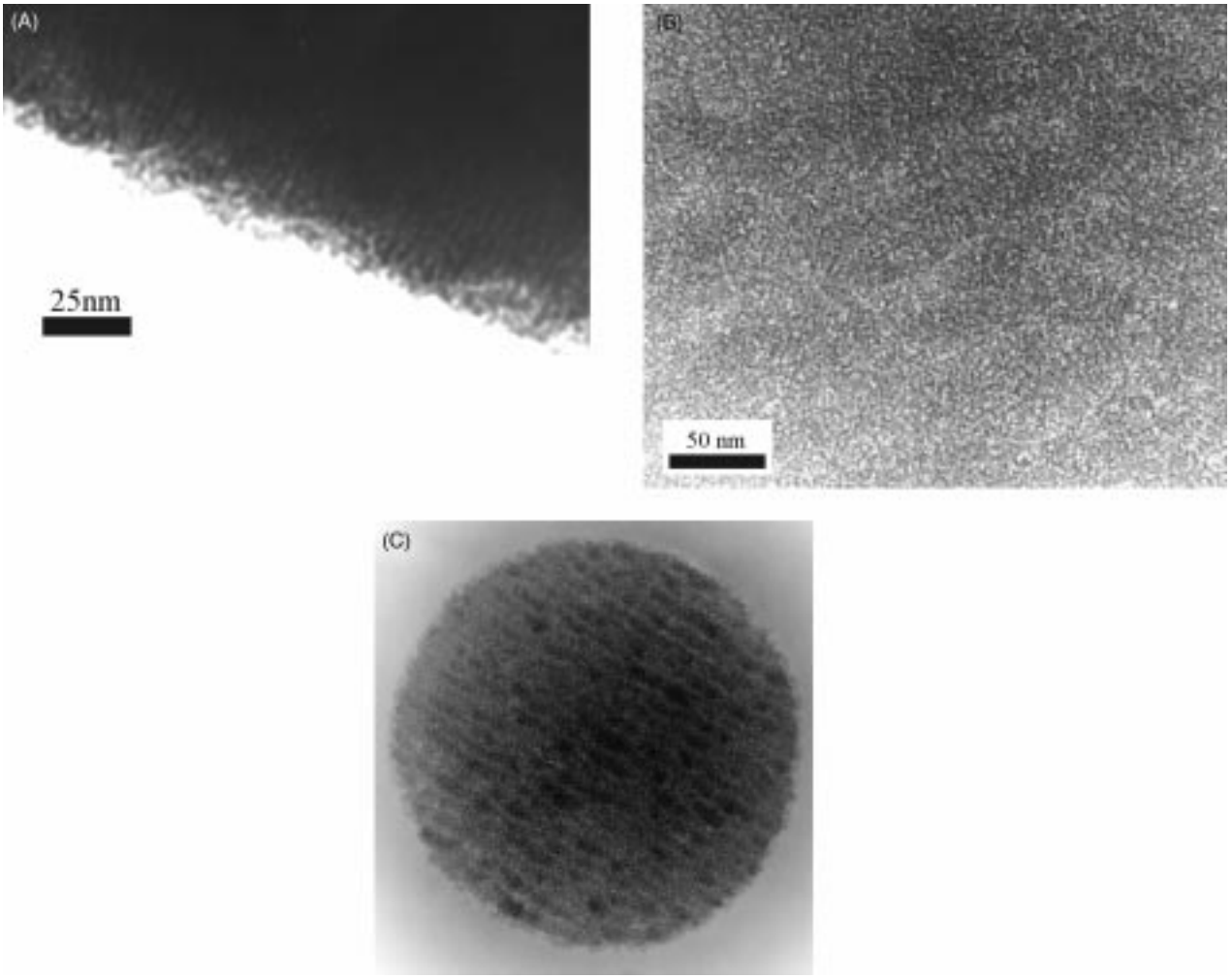

Fig. 4 TEM images (recorded from an epoxy-embedded and microtomed *ca.* 200–500 Å thin section) of microtomed as-synthesized mesoporous spheres in (A) the surface region, (B) center area and (C) a complete sphere

section) for a complete sphere as well as surface and center areas of a sphere are shown in Fig. 4. They reveal a poorly organized mesoporous silica channel plan both in the body and the surface regions of the sphere. The pore center-to-center distance that is estimated from the TEM image is *ca.* 50 Å which agrees with the PXRD results. Since only limited success was achieved in resolving mesopore order in ultrathin *ca.* 200–500 Å sections of the silica spheres, this provides additional evidence that the mesopores are not well ordered.

A selected area electron diffraction (ED) pattern of a thin section of the sphere displays a single diffuse ring with a *d*-spacing of *ca.* 43 Å, Fig. 5, that corresponds to the observed PXRD d_{100}-spacing of *ca.* 45 Å. The diffuse ring ED pattern for the sphere provides further evidence that they have a poorly ordered mesostructure, consistent with PXRD and TEM observations.

Thermogravimetry (TG) traces of the as-synthesized mesoporous silica sphere and gyroid morphologies are shown in Fig. 6. The total mass loss is in the range of 20 to 40 mass% and the thermal transitions below 100 °C, around 300 °C, and above 350 °C respectively correspond to the loss of imbibed water, removal of surfactant, and evolution of water from the condensation–polymerization of residual hydroxy groups in the mesoporous silica.

The trends in the thermal events observed for the spheres are comparable to those of the gyroids made at room temperature and at the same reactant ratio. In both cases, the loss of surfactant at *ca.* 300 °C is the major thermal event, Fig. 6. Noticeably, the mass loss of surfactant from the spheres amounts to *ca.* 20 mass% of the mesoporous silica while that

Fig. 5 A representative electron diffraction pattern of a microtomed as-synthesized mesoporous silica sphere

of the gyroids is *ca.* 40 mass%. This implies that the amount of surfactant in the silicate–surfactant co-assembly that is required to make the spheres is significantly less than that needed to make the gyroids.

Solid state proton decoupled ^{29}Si magic angle spinning nuclear magnetic resonance spectroscopy (^{29}Si MAS NMR) was employed to determine the Q3 (SiO_3OH) : Q4 (SiO_4) ratio of the as-synthesized spheres, Fig. 7. The ratio is *ca.* 0.9 for the

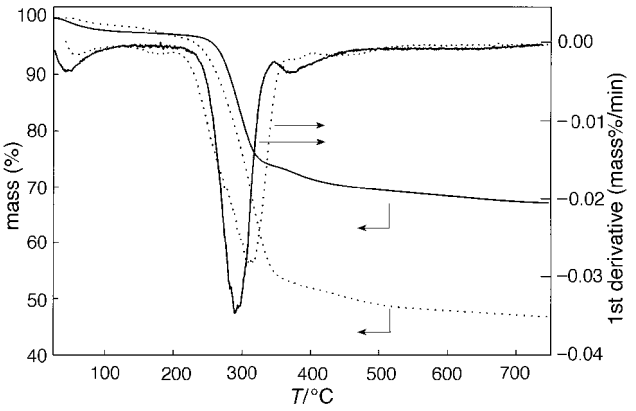

Fig. 6 Representative TG curves for mesoporous spheres (—) and gyroids (---) presented in Fig. 2

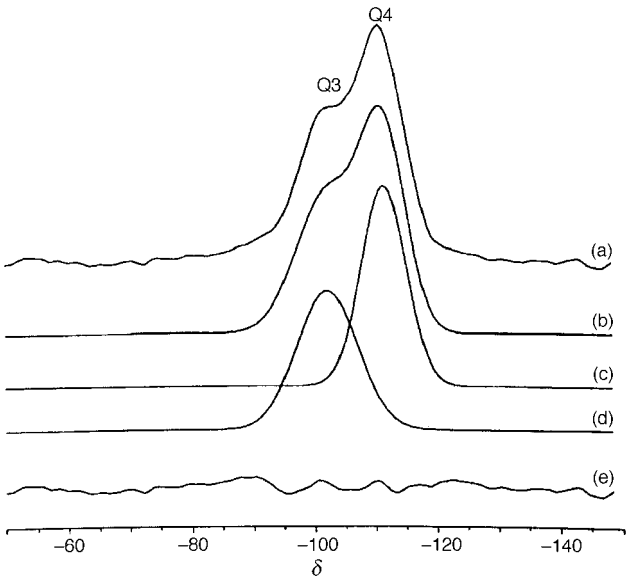

Fig. 7 Solid state proton decoupled ^{29}Si MAS NMR spectra of as-synthesized mesoporous spheres: (a) observed, (b) simulated, (c,d) deconvoluted, (e) difference between observed and simulated. Q3 and Q4 represent $Si(OH)O_3$ and SiO_4 building units that constitute the glassy silica channel walls of the mesostructure.

spheres compared to *ca.* 0.6 for the gyroids, implying a lower degree of silicate polymerization for the spheres.[1,32]

The particle size distribution of the mesoporous silica spheres was measured by using a dynamic light scattering (DLS) analysis technique. The size distribution of the silica mesoporous spheres according to surface area, volume and particle number are found to be unimodal and fall in the micrometer size regime. A distribution curve based on the particle surface area for calcined mesoporous spheres is shown in Fig. 8. The mean diameter for this sample of mesoporous silica spheres is 6.8 μm which agrees well with that observed by SEM, Fig. 2(C).

Nitrogen adsorption isotherms have been recorded at −196 °C for the calcined spheres and gyroids, Fig. 9. They are typical type IV and display an initial steep rise at low partial pressure owing to monolayer nitrogen adsorption in the mesopores (note that, α_s plots show the absence of microporosity), followed by an inflection at higher partial pressure at P/P_0 *ca.* 0.3, arising from capillary condensation of nitrogen in the mesopores.[33] In both cases, there is no hysteresis which suggests that there is negligible obstruction of the channels in both spherical and gyroidal mesoporous silica morphologies, allowing for the reversible adsorption and desorption of nitrogen to take place. Note that the isotherms of these mesoporous

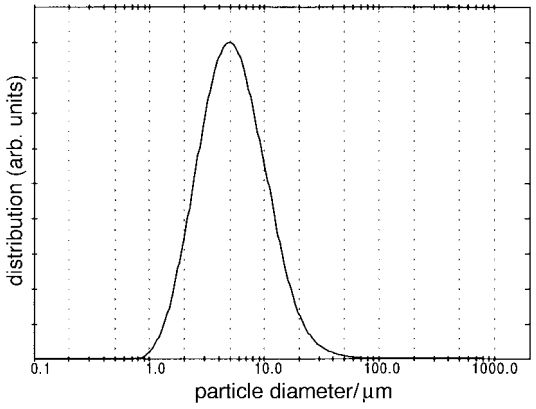

Fig. 8 Particle size distribution of calcined mesoporous spheres based upon particle surface area

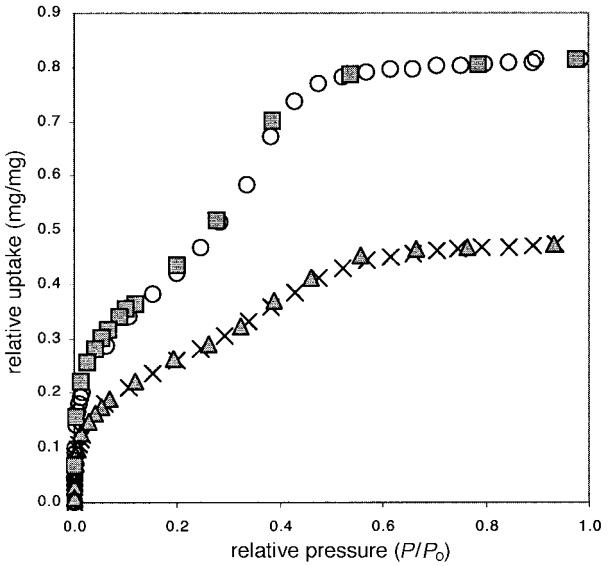

Fig. 9 Nitrogen adsorption isotherms of mesoporous silica sphere (× adsorption, ▲ desorption) and gyroid (○ adsorption, ■ desorption) shapes

silica spheres are distinct from those made by sol–gel hydrolysis approaches, where hysteresis is invariably present on type IV and H2 isotherms.[26,27]

There are obvious differences in the shapes of the isotherms between the spheres and gyroids. The mesoporous silica spheres display a much less steep capillary condensation inflection, indicative of a broader mesopore size distribution. This proposal is confirmed by a Dollimore–Heal analysis of both isotherms[34] which provides estimates for the pore size distribution and the pore volume of the mesoporous silica gyroids and spheres. The surface area was obtained by a standard BET procedure. The adsorption results for the sphere and gyroid shapes are compared in Table 2. The surface area and pore volume of the gyroids are higher than those of the spheres. The width of the pore size distribution at half height for the

Table 2 The surface area, pore volume, mean pore diameter and width of the pore size distribution of mesoporous silica spheres and gyroid shapes made from the same reactant ratios at different temperatures

	BET surface area/$m^2\ g^{-1}$	pore volume /$cm^3\ g^{-1}$	mean pore diameter/Å	full width at half height/Å
sphere	750	0.59	33	19
gyroid	1200	1.01	35	6

gyroids is about three times narrower than that for the spheres, although both have comparable mean pore diameters. These values support the contention from PXRD, ED and TEM that the mesopores in the spheres are not as well organized as in the gyroids.

The sphere syntheses presented so far are for the 80 °C preparations. It is noteworthy that the formation of sphere shaped mesoporous silica depends on both the reactant ratio and temperature. At room temperature and at the same surfactant and TEOS concentrations, the sphere shaped silica can be synthesized at a lower acidity than those synthesized at 80 °C. Several sets of conditions that facilitate sphere formation at room temperature and 80 °C are listed in Table 1. A detailed shape–reactant ratio phase study for different curvature mesoporous silicas, including the sphere shape, is currently underway.

The surface microtopology of the spheres observed by SEM was studied in finer detail by atomic force microscopy (AFM). Interesting structural features were observed on the surface of the mesoporous spheres synthesized at room temperature that were absent for the 80 °C preparations. A contact height mode AFM image of an as-synthesized sphere formed at room temperature reveals a surface with a mottled texture, an average grain size of *ca.* 500–1000 Å, and a mean surface roughness of the same order of magnitude, Fig. 10. The surface of each grain consists of parallel lines with a spacing of *ca.* 70–200 Å but with no clear cross-correlation between the orientation of the mesostructure of the grains. This observation suggests that the sphere may have evolved from the flocculation of silicate liquid crystal seeds that have coalesced in a random fashion and silicified through condensation–polymerization. The surface morphology of the spheres is quite distinct to that of the gyroids where it was found that *ca.* 50–90 Å parallel lines whirl around the unique rotation axis in a manner that mirrors the internal channel architecture.[2]

It is possible to synthetically manipulate the mesoporous silica shapes by changing the acidity, and by employing different reaction temperatures. A catalogue of SEM images that depict representative synthesis-shape transitions induced by increasing the acidity that favors gyroid formation is shown in Fig. 11. The trend is away from gyroids displaying smooth surfaces, to gyroids co-existing with similar shapes but instead exposing surfaces having a multigranular texture, to mixtures of these multigranular shapes but now coexisting with spheres exhibiting smooth surfaces, to purely smooth sphere shapes,

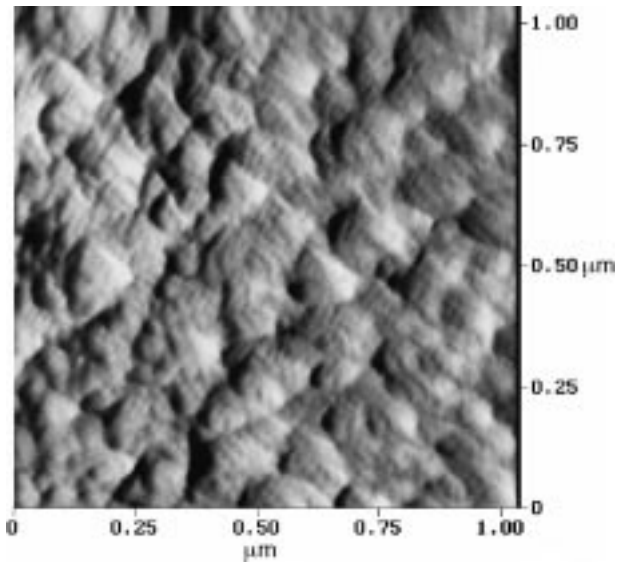

Fig. 10 A representative AFM image of the surface morphology for the as-synthesized mesoporous silica spheres formed at room temperature, showing mesostructured multigranular texture

and ultimately to shapeless forms. By surveying numbers of these morphology changes, it has been found that the multigranular objects that emerge under the varying acidic conditions are in fact composite structures formed from a sheath of grains growing on top of the surface of either a smooth gyroidal or spheroidal central core, Fig. 12. These 'hybrid' morphologies that appear in the gyroid-to-sphere transitional domain might be a manifestation of a growth instability.[35] The PXRD patterns that correspond to the SEM images shown in Fig. 11 depict a transition from well ordered hexagonal mesoporous silica gyroids with sharp low angle reflections, to less ordered channels akin to a 'molten' mesostructure[36] in the spheres with one broad low angle reflection, terminating with dense glassy silica with amorphous form.

It is noteworthy that all of the microscopy, diffraction and spectroscopy measurements performed on the shapeless end-product formed at an even lower acidity in this synthesis system point to a dense and glassy form of silica.

The differences between the sphere and gyroid channel plans, orientational order of the mesopores, thermal behavior, surface area, pore volume and pore size distribution presented here all appear to have a common origin, namely acidity. It is believed that the higher acidic quiescent conditions promote a reaction mechanism based upon the rapid growth and polymerization of a silicate liquid crystal seed, where the curvature arises from local rigidification effects involving the polymerization of the silica.[1,2,9] The chosen acidity conditions with respect to the isoelectric point of silica (pH = 2.0–2.2 at 25 °C),[37] favor protonated silicate precursors and a $SURF^+Cl^-H^+SIL^-$ type of co-assembly,[38] which facilitates the formation of mesoporous silica gyroid shapes with well ordered channels. As the acidity is dropped, the growth process changes from one involving smooth and continuous deposition of silicate–surfactant micellar species onto specific regions of a silicate liquid crystal seed that promote gyroid shapes, to one in which deposition occurs on non-specific regions of the evolving seeds. This creates gyroid morphologies with surfaces comprised of agglomerated grains which under lower acidity conditions metamorphosise to sphere shapes with smooth surfaces. The gyroid shape and channel plan may be initiated by a topological defect comprised of a circular symmetry director field around a liquid crystal defect. By contrast, the lower acidity growth process seems instead to involve a slower and global silicification of a silicate liquid crystal spherical droplet where surface tension determines the final shape of the particle and defects may play a role in determining the channel arrangement. The transformation to the sphere is diagnostic of a shape-transition driven by global surface tension forces of a growing yet slowly polymerizing silicate liquid crystal seed. A soft and evolving mesoporous silica morphology will minimize its surface free energy by forming the shape of a sphere.

The lower acidity synthesis conditions promote the formation of silicates with a lower degree of protonation, lesser charge and fewer charge-balancing surfactants. This leads to a more weakly bound and less well organized surfactant–silicate co-assembly, which silicifies to a less polymerized mesoporous silica sphere, containing less imbibed surfactant than the gyroids as evidenced by TG, and a lower degree of channel order judged by PXRD, ED and TEM data. Under these conditions, the slower polymerization rate makes surface tension the over-riding shape controlling factor. Thus a soft and enlarging mesoporous silica morphology will prefer to assume the shape of a sphere because this minimizes the surface area and surface free energy. By continuing to drop the acidity of the synthesis, one reaches a point where the charge on the silicate precursors is so small that they are unable to sustain any degree of organization with the surfactant micellar assemblies. The result is amorphous and shapeless forms of dense silica.

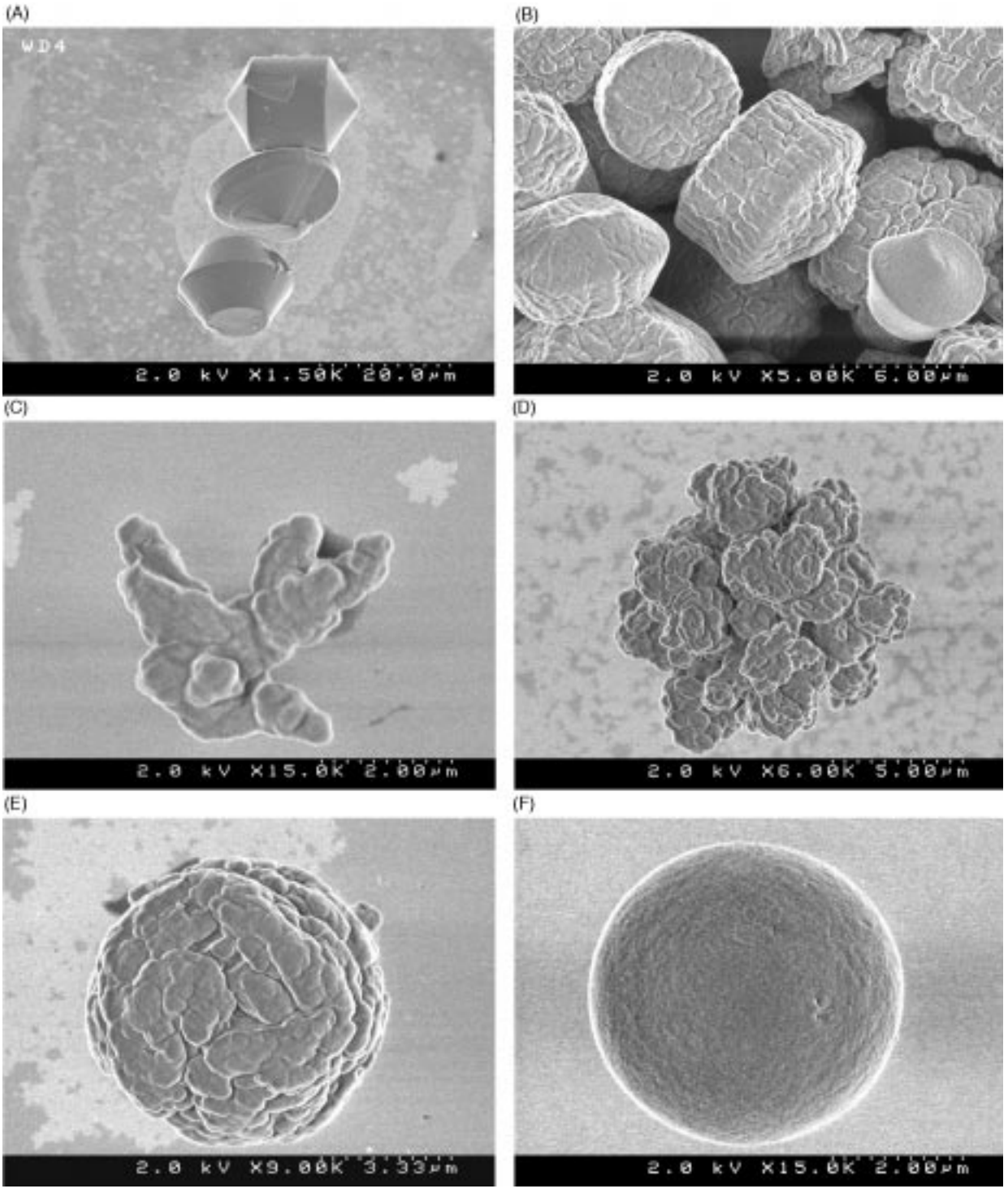

Fig. 11 A series of SEM images illustrating various mesoporous silica shape transitions from (A) gyroids to (F) spheres

Conclusion

The picture that is emerging from our studies of the morphogenesis of shape in hexagonal mesoporous silica[1,2,9] is that there exists a logical relation between the synthesis conditions, polymerization, growth and curvature of a silicate liquid crystal seed, and how this favors a particular morphology. The shape transition of the gyroid to the sphere with the intermediate stage of multigranular 'hybrid' structures is especially interesting because it unveils an acidity and temperature dependent switch in the mode of formation of these morphologies, indicative of reaction instabilities. It appears that the higher acidity growth process that captures gyroid shapes with the channels arranged concentrically around the unique rotation axis involves rapid and local silicification and curvature of an evolving silicate liquid crystal seed, possible initiated by a liquid crystal defect. By contrast, the lower acidity circumstances favor a slower and spatially more extensive silicification process in which colloidal and surface tension forces dominate and promote sphere formation.

Financial support from Mobil Technology Company is deeply appreciated. Technical discussions with Dr Charles Kresge proved to be invaluable. H.Y. is grateful for an Ontario Graduate Scholarship held during this research. We thank Dr Dmitri Rubisov for conducting the particle size distribution experiments and analyzing the data. The assistance of Dr Patricia Aroca with the recording of solid state ^{29}Si MAS NMR spectra proved to be beneficial. Permission to use the

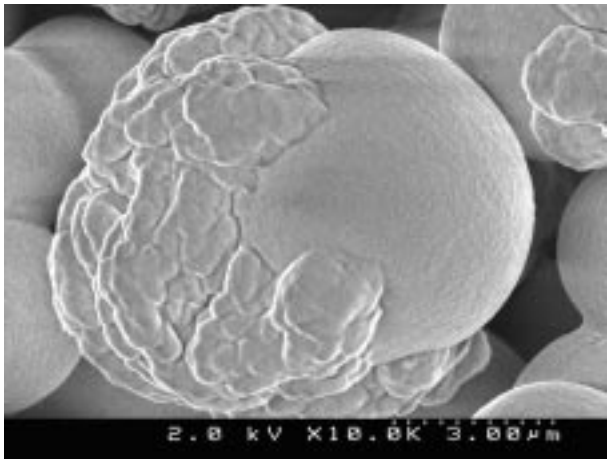

Fig. 12 Example of a hybrid mesoporous silica morphology built of a sheath of grains growing on top of the surface of a smoother spheroidal central core

AFM equipment of Dr Grant S. Henderson in Geology at the U of T is deeply appreciated.

References

1 H. Yang, N. Coombs and G. A. Ozin, *Nature (London)*, 1997, **386**, 692.
2 G. A. Ozin, H. Yang, I. Sokolov and N. Coombs, *Adv. Mater*., 1997, **9**, 662.
3 H. Yang, A. Kuperman, N. Coombs, N. Mamiche-Afara and G. A. Ozin, *Nature (London)*, 1996, **379**, 703.
4 G. A. Ozin, D. Khushalani and H. Yang, in *Proceedings of the NATO Advanced Research Workshop on 'Molecular Recognition'*, ed. J. Wuest, Val Morin, May 1996, Kluwer Academic Publications, Dordrecht, in press.
5 H. Yang, N. Coombs, I. Sokolov and G. A. Ozin, *J. Mater. Chem*., 1997, **7**, 1285.
6 H. Yang, N. Coombs, I. Sokolov and G. A. Ozin, *Nature (London)*, 1996, **381**, 589.
7 H. Yang, N. Coombs, Ö. Dag, I. Sokolov and G. A. Ozin, *J. Mater. Chem*., 1997, **7**, 1755.
8 H. Yang, N. Coombs and G. A. Ozin, *Adv. Mater*., 1997, **9**, 811.
9 N. Coombs, D. Khushalani, S. Oliver, G. A. Ozin, G. C. Shen, I. Sokolov and H. Yang, *J. Chem. Soc., Dalton Trans*., 1997, 3941.
10 C. T. Kresge, M. E. Leonowicz, W. J. Roth, J. C. Vartuli and J. C. Beck, *Nature (London)*, 1992, **359**, 710.
11 J. S. Beck, J. C. Vartuli, W. J. Roth, M. E. Leonowicz, C. T. Kresge, K. T. Schmitt, C. T.-W. Chu, D. H. Olson, E. W. Sheppard, S. B. McCullen, J. B. Higgins and J. L. Schlenker, *J. Am. Chem. Soc*.., 1992, **114**, 10 834.
12 F. Di Renzo, H. Cambon and R. Dutartre, *Microporous Mater*., 1997, **10**, 283, history behind the discovery of the surfactant-based synthesis of periodic mesoporous silica.[10,11]
13 S. Mann and G. A. Ozin, *Nature (London)*, 1996, **382**, 313.
14 Q. Huo, J. Feng, F. Schüth and G. D. Stucky, *Chem. Mater*., 1997, **9**, 14.
15 M. Grün, I. Lauer and K. K. Unger, *Adv. Mater*., 1997, **9**, 254.
16 (*a*) I. A. Aksay, M. Trau, S. Manne, I. Honma, N. Yao, L. Zhou, P. Fenter, P. M. Eisenberger and S. M. Gruner, *Science*, 1996, **273**, 892; (*b*) H. W. Hillhouse, T. Okubo, J. W. van Egmond and M. Tsapatsis, *Chem. Mater*., 1997, **9**, 1505.
17 M. Ogawa, *J. Am. Chem. Soc*., 1994, **116**, 7941.
18 M. Ogawa, *Chem. Commun*., 1996, 1149.
19 Y. Lu, R. Ganguli, C. A. Drewien, M. T. Anderson, C. J. Brinker, W. Gong, Y. Guo, H. Soyez, B. Dunn, M. H. Huang and J. I. Zink, *Nature (London)*, 1997, **389**, 364.
20 (*a*) Schacht, Q. Huo, I. G. Voigt-Martin, G. D. Stucky and F. Schüth, *Science*, 1996, **273**, 768; (*b*) S. H. Tolbert, T. E. Schäffer, J. Feng, P. K. Hansma and G. D. Stucky, *Chem. Mater*., 1997, **9**, 1962.
21 (*a*) H.-P. Lin and C.-Y. Mou, *Science*, 1996, **273**, 765; (*b*) M. R. Raimondi, T. Maschmeyer, R. H. Templer and J. M. Seddon, *Chem. Commun*., 1997, 1843; (*c*) M. Trav, N. Yao, E. Kim, Y. Xia, G. M. Whitesides and I. A. Aksay, *Nature* (*London*), 1997, **390**, 674.
22 E. Matijevic, *Curr. Opin. Colloid Interface Sci*., 1996, **1**, 176 and references therein.
23 E. Matijevic, *Pure Appl. Chem*., 1988, **60**, 1479.
24 C. J. Brinker and G. W. Scherer, *Sol-Gel Science*, Academic Press, San Diego, CA, 1990.
25 M. A. Bulter, P. F. James and J. D. Jackson, *J. Mater. Sci*., 1996, **31**, 1675.
26 H. Izutsu, F. Mizukami, P. K. Nair, Y. Kiyozumi and K. Maeda, *J. Mater. Chem*., 1997, **7**, 767.
27 L. C. Klein and R. H. Woodman, in *Sol–Gel Science and Technology*, ed. E. J. A. Pope, S. Sakka and L. C. Klein, The American Ceramic Society, Westerville, OH, 1995, pp. 105–116.
28 B. Karmakar, G. De, D. Kundu and D. Ganguli, *J. Non-Cryst. Solids*, 1991, **135**, 29.
29 T. Tanev and T. J. Pinnavaia, *Science*, 1995, **267**, 865.
30 A. Bagshaw, E. Prouzet and T. J. Pinnavaia, *Science*, 1995, **269**, 1242.
31 A. Firouzi, F. Atef, A. G. Oertli, G. D. Stucky and B. F. Chmekla, *J. Am. Chem. Soc*., 1997, **119**, 3596.
32 A. Steel, S. W. Carr and M. W. Anderson, *Chem. Mater*., 1995, **7**, 1829.
33 S. J. Gregg and K. S. W. Sing, *Adsorption, Surface Area and Porosity*, Academic Press, London, 2nd edn., 1982, p. 113.
34 D. Dollimore and G. R. Heal, *J. Appl. Chem*., 1964, **14**, 109.
35 *Chemical Waves and Patterns*, ed. R. Kapral and K. Showalter, Kluwer Academic, Dordrecht, The Netherlands, 1995.
36 S. T. Hyde, *Curr. Opin. Solid State Mater. Sci*., 1996, **1**, 653.
37 R. K. Iler, *The Chemistry of Silica*, John Wiley & Sons, New York, 1979, pp. 180–189.
38 Q. Huo, D. I. Margolese, U. Ciesla, D. G. Demuth, P. Feng, T. E. Gier, P. Sieger, A. Firouzi, B. F. Chmekla, F. Schuth and G. D. Stucky, *Chem. Mater*., 1994, **6**, 1176.

Paper 7/05746F; *Received* 6*th August*, 1997